BIOCHEMISTRY
including biophysical chemistry & molecular biology

Article

pubs.acs.org/biochemistry

Interaction with the Redox Cofactor MYW and Functional Role of a Mobile Arginine in Eukaryotic Catalase-Peroxidase

Bernhard Gasselhuber,[†] Michael M. H. Graf,[‡] Christa Jakopitsch,[†] Marcel Zamocky,[†,∥] Andrea Nicolussi,[†] Paul G. Furtmüller,[†] Chris Oostenbrink,[‡] Xavi Carpena,[§] and Christian Obinger*[,†]

[†]Department of Chemistry, Division of Biochemistry, BOKU-University of Natural Resources and Life Sciences, Muthgasse 18, A-1190 Vienna, Austria

[‡]Department of Material Sciences and Process Engineering, Institute for Molecular Modeling and Simulation, BOKU-University of Natural Resources and Life Sciences, Muthgasse 18, A-1190 Vienna, Austria

[§]Institut de Biologia Molecular (IBMB-CSIC), Parc Cientific de Barcelona, Baldiri Reixac 10-12, 08028 Barcelona, Spain

[∥]Institute of Molecular Biology, Slovak Academy of Sciences, Dubravska cesta 21, SK-84551 Bratislava, Slovakia

Supporting Information

ABSTRACT: Catalase-peroxidases (KatGs) are unique bifunctional heme peroxidases with an additional posttranslationally formed redox-active Met-Tyr-Trp cofactor that is essential for catalase activity. On the basis of studies of bacterial KatGs, controversial mechanisms of hydrogen peroxide oxidation were proposed. The recent discovery of eukaryotic KatGs with differing pH optima of catalase activity now allows us to scrutinize those postulated reaction mechanisms. In our study, secreted KatG from the fungus *Magnaporthe grisea* (*Mag*KatG2) was used to analyze the role of a remote KatG-typical mobile arginine that was shown to interact with the Met-Tyr-Trp adduct in a pH-dependent manner in bacterial KatGs. Here we present crystal structures of *Mag*KatG2 at pH 3.0, 5.5, and 7.0 and investigate the mobility of Arg461 by molecular dynamics simulation. Data suggest that at pH ≥4.5 Arg461 mostly interacts with the deprotonated adduct Tyr. Elimination of Arg461 by mutation to Ala slightly increases the thermal stability but does not alter the active site architecture or the kinetics of cyanide binding. However, the variant Arg461Ala lost the wild-type-typical optimum of catalase activity at pH 5.25 (k_{cat} = 6450 s^{-1}) but exhibits a broad plateau between pH 4.5 and 7.5 (k_{cat} = 270 s^{-1} at pH 5.5). Moreover, significant differences in the kinetics of interconversion of redox intermediates of wild-type and mutant protein mixed with either peroxyacetic acid or hydrogen peroxide are observed. These findings together with published data from bacterial KatGs allow us to propose a role of Arg461 in the H_2O_2 oxidation reaction of KatG.

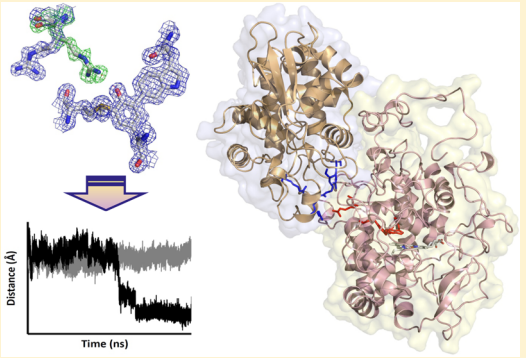

Recently, the first structures of a eukaryotic bifunctional catalase-peroxidase (KatGs) in the ferric resting[1] and oxoiron[2] state were published. Similar to the prokaryotic counterparts,[3−7] eukaryotic KatGs have two interdependent cooperating redox-active cofactors at their active site, namely a heme *b* and a unique posttranslationally and autocatalytically formed Met299-Tyr273-Trp140 (MYW) adduct [extracellular *Magnaporthe grisea* KatG (*Mag*KatG2) numbering throughout]. KatG can be described as a catalase in peroxidase clothing[8] because it has been engineered by Nature to catalyze efficient H_2O_2 dismutation similar to monofunctional catalases.[9,10] Together with cytochrome *c* peroxidases, ascorbate peroxidases and hybrid-type peroxidases KatGs comprise Family I of the peroxidase-catalase superfamily.[11,12] Besides the MYW adduct mentioned above, further KatG-specific structural peculiarities include (i) a two-domain structure with only the N-terminal domain containing the two redox cofactors and essential catalytic residues,[1,3,4] (ii) loop insertions that contribute to the architecture of the long and restricted access channel, and (iii) a fully conserved aspartate at the entrance of the substrate channel to the heme cavity.[13,14] Mutation of any of these KatG-typical structural features typically reduces the catalase activity without compromising the peroxidase activity.[13−22]

Both the heme and the Met299-Tyr273-Trp140 cofactor found in KatG are mutually dependent on one another to support efficient H_2O_2 dismutation. On the basis of (i) time-resolved spectroscopic studies, including freeze-quench electron paramagnetic resonance (EPR) spectroscopies, and (ii) hybrid quantum mechanics/molecular mechanics (QM/MM) computational studies, the following sequence of reactions has been proposed to account for the *catalatic* activity of KatG (see also Supplemental Figure 1).[14,17−19,23−27] Initially, ferric KatG [MYW···Fe(III) Por] is oxidized by hydrogen peroxide to Compound I [MYW···Fe(IV)═O $Por^{+\bullet}$], which is typical of

Received: May 3, 2016
Revised: June 4, 2016
Published: June 13, 2016

DOI: 10.1021/acs.biochem.6b00436
Biochemistry 2016, 55, 3528−3541

monofunctional peroxidases and catalases (reaction I).[25,28,29] However, in KatG, the porphyryl radical is rapidly quenched by an internal electron-transfer process producing oxoiron(IV) and the adduct radical ($MYW^{+\bullet}$) (reaction II).[14,23,24] This Compound I* [$MYW^{+\bullet}\cdots Fe(IV)-OH$ Por] reacts with the second H_2O_2 in a nonscrambling mechanism[30] to directly form Compound III* (reaction III), a dioxyheme intermediate with distinct spectral features that may be considered analogous to oxymyoglobin, oxyhemoglobin, and peroxidase Compound III as a complex between ferrous heme and dioxygen [$Fe(II)-O_2$], which is isoelectronic with superoxide bound to ferric heme [$Fe(III)-O_2^{-\bullet}$].[31] Monofunctional peroxidases have negligible catalase activity and are trapped in this Compound III state in the presence of H_2O_2 only.[31] However, in KatG, the superoxyferric complex is formed in the presence of the adduct radical (i.e., Compound III*)[14,19,24] (reaction III), thereby keeping an oxidation equivalent very close to superoxide in the $Fe(III)-O_2^{-\bullet}$ complex, which is the dominating electronic structure during KatG turnover.[27] This guarantees rapid decomposition of Compound III* to the ferric resting state, thereby releasing solely triplet oxygen.[23] The balance of one KatG turnover is dismutation of hydrogen peroxide ($2H_2O_2 \rightarrow 2H_2O + O_2$), which is exactly the same as in monofunctional catalases. However, the mechanism of reaction is completely different and clearly reflects the fact that KatG is a posttranslationally modified peroxidase with a dominating *catalatic* besides a conventional peroxidase activity. With regard to reactions III and IV, an alternative mechanism has been postulated,[26] including the transfer of (i) a hydrogen atom from the second H_2O_2 molecule to the oxyferryl species of Compound I* producing the hydroperoxide radical and restoring the ferric state as well as (ii) a proton from the adduct tryptophan to the [Fe(III)−OH] state thereby releasing water.[26]

$$[MYW\cdots Fe(III)\ Por] + H_2O_2 \rightarrow [MYW\cdots Fe(IV)=O\ Por^{+\bullet}] + H_2O \quad (I)$$

$$[MYW\cdots Fe(IV)=O\ Por^{+\bullet}] + H^+ \rightarrow [MYW^{+\bullet}\cdots Fe(IV)-OH\ Por] \quad (II)$$

$$[MYW^{+\bullet}\cdots Fe(IV)-OH\ Por] + H_2O_2 \rightarrow H^+ + H_2O + \{[MYW^{+\bullet}\cdots Fe(II)-O_2\ Por] \leftrightarrow [MYW^{+\bullet}\cdots Fe(III)-O_2^{-\bullet}\ Por]\} \quad (III)$$

$$[MYW^{+\bullet}\cdots Fe(III)-O_2^{-\bullet}\ Por] \rightarrow [MYW\cdots Fe(III)\ Por] + O_2 \quad (IV)$$

Interestingly, the chemical properties of the KatG-typical adduct seem to be modulated by a fully conserved mobile arginine residue far from the heme (~20 Å) but closely related to the adduct. X-ray structures of bacterial KatGs showed that the Arg can switch between two distinct conformations ("in" vs "out") depending on pH. Below pH 6.5 (i.e., the pH optimum of catalase activity as well as the proposed pK_a of the adduct tyrosine in prokaryotic KatGs), the out conformation dominates, whereas under alkaline conditions, Arg points predominantly toward the adduct and forms an ionic interaction with the tyrosinate of the adduct. Elimination of this basic amino acid strongly reduces the catalase activity but not the peroxidase activity of KatG.[14,33,34]

Although several years of elaborate research have passed, there are still open questions about the *catalatic* reaction of KatGs. The recent finding that eukaryotic *Mag*KatG2 has some novel structural features[1,2,35] and a more acidic pH optimum (i.e., pH 5.25) for H_2O_2 dismutation[36] now allows us to scrutinize whether the postulated *catalatic* mechanism (reactions I−IV) and the role of the mobile arginine in modulating the pH dependence are also valid for eukaryotic KatGs. In this work, we have determined the X-ray structures of *Mag*KatG2 at pH 3, 5.5, and 7.0 and investigated the dynamics of Arg461 in ferric *Mag*KatG2 by molecular dynamics simulation. We demonstrate the effect of exchange of Arg461 with alanine on active site geometry, thermal stability, and ligand binding as well as on the pH dependence of bifunctional activity. Furthermore, the kinetics of peroxyacetic acid- and H_2O_2-mediated interconversion of redox intermediates of wild-type *Mag*KatG2 and the variant Arg461Ala are presented, discussed, and compared with those reported for prokaryotic catalase-peroxidases.

MATERIALS AND METHODS

Site-Directed Mutagenesis, Heterologous Expression, and Protein Purification. Mutagenesis of the recombinant extracellular catalase-peroxidase from *M. grisea* and expression of the wild-type and mutant protein in *Escherichia coli* strain BL21(DE3) Star (Invitrogen) were performed as described recently.[1,2] Briefly, the point mutation was introduced with a polymerase chain reaction-based site-directed mutagenesis kit (QuikChange Lightning Kit from Agilent Technologies) using two complementary oligonucleotides with the planned mutation in the middle of their sequence (5′-AACTGCTGC-ATGCTGATCTGGGCCCGACCACC-3′ and 3′-GGTGGT-CGGGCCCAGATCAGCATGCAGCAGTTT-5′). For protein expression, transformed *E. coli* cells were grown in M9ZB medium [supplemented with ampicillin (100 μg mL^{-1})] and 40 mg L^{-1} hemin prior to induction. After induction by 0.5% (w/v) lactose or 0.5 mM isopropyl β-D-1-thiogalactopyranoside, the cultivation temperature was lowered to 16 °C during overnight protein expression. Cells were harvested by centrifugation and homogenized by multiple ultrasonication cycles. The crude homogenate was clarified by centrifugation (>20000*g*), and the clear supernatant was loaded onto a 20 mL Chelating Sepharose Fast Flow Column (GE Healthcare). His-tagged proteins were eluted with a linearly increasing gradient of imidazole and immediately checked by UV−vis spectroscopy. The KatG-containing fractions were pooled, concentrated by centrifugation, and further purified using a hydroxyapatite column (25 mL, Bio-Rad) following a stepwise elution [step 1 being 50 mM phosphate buffer (pH 7.7) and then step 2 being 200 mM phosphate buffer (pH 8.0)].

For evaluation of purification success, protein electrophoresis was performed with NuPAGE Novex Bis-Tris gradient gels (4 to 12%) with 15 wells (Invitrogen) (running buffer being MOPS with SDS). Gels were stained with Coomassie Brilliant Blue (Sigma-Aldrich) or immunoblotted onto a nitrocellulose membrane (Amersham Biosciences) for detection of *Mag*KatG2 by using a penta-His antibody.

Protein Crystallization, Data Collection, and Structure Determination. Crystals of poly-His-tagged *Mag*KatG2 were obtained using the sitting-drop vapor-diffusion method at 4 °C with a protein concentration of 5 mg/mL in 5 mM phosphate buffer (pH 7.5). The mother liquor contained 15% PEG 4000 and 0.1 M sodium acetate (pH 4.6). Crystals were soaked in

DOI: 10.1021/acs.biochem.6b00436
Biochemistry 2016, 55, 3528−3541

Table 1. Data Collection and Structural Refinement Statistics for *Mag*KatG2 at Different pH Values

	pH 3	pH 5.5	pH 7
		Data Collection	
space group	$P2_12_12_1$	$P2_12_12_1$	$P2_12_12_1$
unit cell parameters [*a*, *b*, *c* (Å)]	103.2, 109.9, 132.1	103.8, 109.7, 134.1	103.2, 109.4, 133.4
resolution (Å)	30−1.4 (1.44−1.40)	30−1.4 (1.44−1.40)	30−1.7 (1.74−1.70)
no. of unique reflections	293409 (21354)	284103 (21506)	161673 (11750)
completeness (%)	99.9 (98.9)	94.9 (97.8)	97.5 (96.6)
R_{sym} (%)	6.4 (52.7)	7.2 (37.7)	6.6 (51.9)
R_{meas} (%)	7.0 (57.7)	8.2 (44.0)	7.5 (58.3)
$\langle I/\sigma I \rangle$	16.2 (3.4)	10.6 (2.8)	14.6 (2.7)
redundancy	6.6 (6.0)	3.9 (3.6)	4.6 (4.7)
		Model Refinement	
resolution (Å)	20−1.4 (1.44−1.40)	20−1.4 (1.44−1.40)	20−1.7 (1.74−1.70)
no. of reflections	278676 (20157)	269831 (20318)	153550 (11090)
no. of free reflections	13911 (1092)	14260 (1087)	8122 (581)
R_{cryst} (%)	13.8 (19.8)	15.1 (20.8)	15.6 (21.0)
R_{free} (%)	16.1 (22.9)	17.6 (25.5)	18.6 (24.6)
no. of residues	1469	1469	1470
no. of waters	1749	1799	1701
no. of ligands	2	2	2
average *B* factor (Å^2)			
protein	15.6	13.9	19.9
ligands	10.4	9.4	14.5
water	26.7	22.9	28.5
all atoms	17.1	15.1	21.0
root-mean-square deviation			
bond lengths (Å)	2.8×10^{-2}	2.7×10^{-2}	1.1×10^{-2}
bond angles (deg)	2.50	2.35	1.44

buffers with varying pH values (phosphate-citrate or phosphate) containing elevated levels of PEG 4000 (35%) as a cryoprotectant. At beamline ID23eh1 (ESRF, Grenoble, France), diffraction data up to 1.4 Å were obtained using flash-cooled crystals. Crystals belonged to space group $P2_12_12_1$, and a biological dimer was present in the asymmetric unit. A molecular replacement solution was found for the newly obtained data sets using the wild-type structure of *Mag*KatG2 [Protein Data Bank (PDB) entry 3UT2] as a search model. Data collection and structural refinement statistics for all presented structures are summarized in Table 1. Structure factors and coordinates have been deposited in the Protein Data Bank as entries 5JHX, 5JHY, and 5JHZ.

UV−Vis and Electronic Circular Dichroism Spectroscopy. UV−visible spectra of wild-type *Mag*KatG2 and its variants were routinely recorded with a Hitachi U-3900 spectrophotometer at 25 °C. The molar absorption coefficient of the ferric, high-spin *Mag*KatG2 at Soret maximum (ε_{404} = 102600 M^{-1} cm^{-1}) was determined recently[2] and used for calculation of KatG concentrations throughout this work. The absorption coefficient of *Mag*KatG2 at 280 nm (ε_{280}) was calculated to be 147800 M^{-1} cm^{-1} using the protein sequence (Expasy server). The spectra were recorded in either 50 mM citrate-phosphate buffer (pH 4.0−5.5) or 50 mM phosphate buffer (pH 7.0−8.5).

Electronic circular dichroism (ECD) spectra were recorded on a Chirascan spectrophotometer (Applied Photophysics, Leatherhead, U.K.). The instrument was flushed with nitrogen with a flow rate of 5 L min^{-1}. The instrument allowed simultaneous UV−vis and ECD monitoring and was equipped with a Peltier element for temperature control. For recording of far-UV spectra (260−190 nm), the quartz cuvette had a path length of 1 mm, and for recording visible spectra, a path length of 10 mm was used. Instrumental parameters were set as follows: spectral bandwidth, 5 nm; step size, 1 nm; scan time, 15 s per point.

To monitor the thermal unfolding, 5 μM wild-type or mutant KatGs were incubated in 5 mM phosphate buffer (pH 7.0) with a stepwise increasing temperature (1 °C min^{-1}) ranging from 20 to 90 °C. Single-wavelength scans were performed with instrumental parameters set as follows: spectral bandwidth, 1 mm (Soret) or 0.5 mm (far-UV); scan time per point, 12 s. Melting temperatures (T_m) were determined by sigmoidal fitting of obtained graphs using Pro-Data Viewer from Applied Photophysics (version 4.1.9).

Differential Scanning Calorimetry. Thermal denaturation of *Mag*KatG2 and its variant was monitored using a VP-DSC MicroCal LLC calorimeter from GE Healthcare. The machine uses a cell volume of 137 μL and is equipped with a cooled autosampler for 96-well plates and automated cell cleaning and sample injection. The protein concentration of all samples was 5 μM in 5 mM phosphate buffer (pH 7.0−8.5) or 5 mM citrate-phosphate buffer (pH 4.5−5.5). The differential heat capacity (ΔC_p) was recorded between 20 and 90 °C with a heating rate of 60 °C h^{-1}. Baseline correction of the recorded thermograms was done by subtraction of buffer runs or rescans of each respective sample. After normalization for the exact protein concentrations, the acquired peaks were fitted by a non-two-state unfolding model using the LLC-Cap-DSC Add-on of Origin 7.0 (OriginLab).

***Catalatic* and Peroxidatic Activity Measurements.** Apparent kinetic parameters of catalase activity were determined polarographically using a Clark-type electrode from Hansatech (Oxygraph plus). The temperature was held

DOI: 10.1021/acs.biochem.6b00436
Biochemistry 2016, 55, 3528−3541

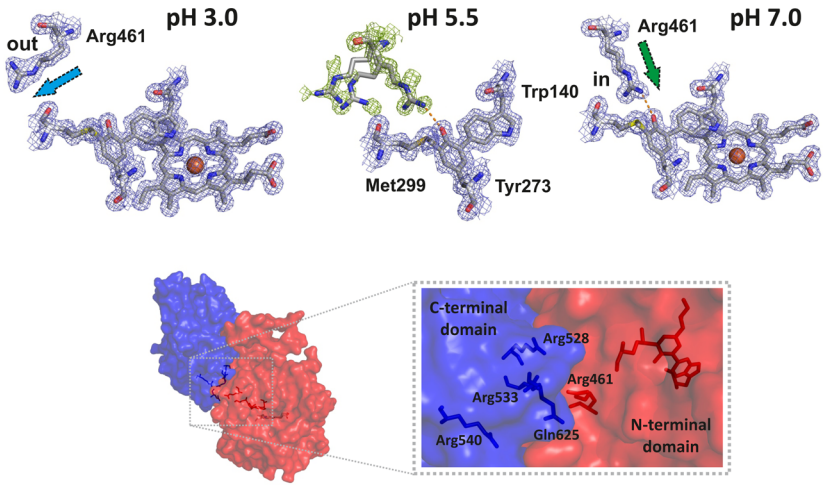

Figure 1. Crystal structures of wild-type *Mag*KatG2 soaked at pH 3.0, 5.5, and 7.0. Representations of pH 3.0 and 7.0 include heme, a covalent adduct, and mobile Arg461. The electron density map drawn at σ = 1.0 shows two possible conformations of Arg461. The acidic environment (pH 3.0) gives 100% "out" conformation, whereas at pH 7.0, 100% "in" conformation is seen. At pH 5.5, both conformations are present. The bottom panel shows the two-domain structure of a *Mag*KatG2 monomer with the heme containing domain colored red and the C-terminal domain blue. In its "out" conformation, Arg461 interacts solely with residues from the C-terminal domain close to a conserved region containing three arginines. Figures were created with PyMOL (PyMOL Molecular Graphics System, version 1.3.0, Schrödinger, LLC, Portland, OR).

constant at 30 °C by a thermostat-controlled water bath. The electrode was equilibrated by flushing the stirred reaction chamber with either dioxygen (O_2) (100% saturation) or pure nitrogen (N_2) (0% saturation). Reactions were started in oxygen-free 50 mM citrate-phosphate (pH 4.0−7.0) or 50 mM phosphate buffer (pH 7.0−8.5) by addition of enzyme. One unit of catalase activity was defined as the amount of enzymes that decomposes 1 μmol of hydrogen peroxide per minute in a 5 mM hydrogen peroxide solution at 30 °C. Final protein concentrations were 1 and 10 nM for the wild-type enzyme and Arg461Ala variant, respectively.

Peroxidatic activity was monitored spectrophotometrically at 470 nm by using 1 mM peroxyacetic acid or hydrogen peroxide as oxidants and guaiacol (ε_{470} = 26.6 M^{-1} cm^{-1}) as the one-electron donor (1 mM) (all from Sigma-Aldrich). One unit of peroxidase activity was defined as the amount of enzyme that oxidizes 1 μmol of selected electron donor per minute at room temperature (25 °C).

Stopped-Flow Spectroscopy. Kinetic measurements of the direct reaction between the ferric proteins with cyanide, hydrogen peroxide, and peroxyacetic acid (PAA) at 25 °C were performed using SX-18MV or Pi*-180 stopped-flow machines from Applied Photophysics. Diluted PAA solutions were routinely incubated with low nanomolar concentrations of bovine liver catalase for degradation of H_2O_2. The path length of the optical cells was 10 mm and the volume 20 μL. Peroxide solutions were prepared freshly and diluted in 50 mM citrate-phosphate (pH 4.0−7.0) or 50 mM phosphate buffer (pH 7.0−8.5).

Calculation of pseudo-first-order rate constants (k_{obs}) was performed with the Pro-Data Viewer software (Applied Photophysics, version 4.1.9). Second-order rate constants were determined from plots of k_{obs} versus substrate concentration.

Molecular Dynamics Simulations. Molecular dynamics simulations of a *Mag*KatG2 monomer (PDB entry 3UT2[1]) were performed using the GROMOS11 software package[37] with the 54A7 force field.[38] The simulations were conducted for 50 ns at a constant temperature (300 K) and a constant pressure (1 atm) and essentially performed as described previously.[2] In the work presented here, the aim was to study the effect of the protonation state of the Tyr273 side chain on the conformational preference of mobile Arg461. Consequently, we conducted the following four independent MD simulations with Tyr273 either protonated (HO-Tyr273) or deprotonated ($^-$O-Tyr273) and Arg461 in the "in" or "out" conformation: HO-Tyr/Arg"out", HO-Tyr/Arg"in", $^-$O-Tyr/Arg"out", and $^-$O-Tyr/Arg"in".

The relative free energies of the mobile Arg461 were calculated according to the linear interaction energy (LIE) method using the following equation:[39]

$$\Delta G = \beta(\langle V^{EL}\rangle_{end} - \langle V^{EL}\rangle_{start}) + \alpha(\langle V^{VdW}\rangle_{end} - \langle V^{VdW}\rangle_{start}) \quad (1)$$

where angular brackets indicate ensemble averages, calculated over one of the four simulations. V^{EL} and V^{VdW} represent the electrostatic and van der Waals interactions, respectively. The subscripts start and end refer to hypothetical processes involving protonation of Tyr273 and a conformational change of Arg461 from the "out" to the "in" conformation, respectively. β and α are parameters of the LIE equation and were set to 0.5 and 0.18, respectively.[40,41] Figure 3 graphically depicts the processes that were studied. Only the first 10 ns of the four simulations were used for the free energy estimates because Arg461 changed its conformation from "out" to "in" in simulation $^-$O-Tyr/Arg"out" afterward.

RESULTS

X-ray Structures of Wild-Type *Mag*KatG2 at pH 3, 5.5, and 7.0. Before analysis of the functional role of Arg461 in ferric *Mag*KatG2, we aimed to investigate its conformation in protein crystals at various pH values. In prokaryotic KatGs crystallized so far, this mobile amino acid showed a clear sensitivity to pH with mixed conformations around pH 6.0, 100% "out" conformation at pH <5, and 100% "in" conformation at pH >7.0.[3,4,7,32] Crystals of *Mag*KatG2 were obtained using the sitting-drop vapor-diffusion method at pH

DOI: 10.1021/acs.biochem.6b00436
Biochemistry 2016, 55, 3528−3541

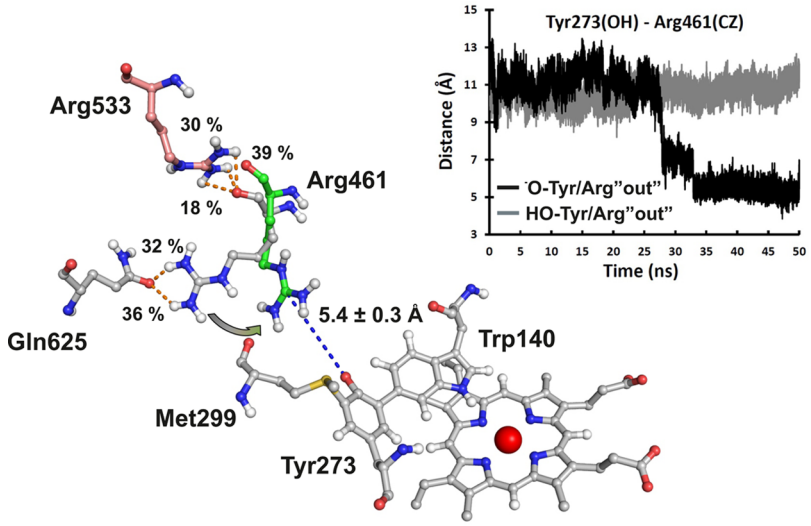

Figure 2. MD simulations for two different protonation states of Tyr273. In both cases, the simulation starts with the "out" conformation of Arg461. The left panel shows the two redox cofactors heme *b* and the Trp140-Tyr273-Met299 adduct and Arg461 in two conformations [i.e., snapshots at 0 ns (white) and 50 ns (green) simulation of starting model ⁻O-Tyr/Arg"out"], including the interaction partners Arg533 and Gln625. Calculated hydrogen bonding between Arg461 and Arg533 as well as Gln625 is given in percent occurrence for the 50 ns simulation. The right panel shows the changes in distance between the tyrosinate oxygen and the guanidinium carbon of Arg461 during simulation for the two models considered: gray line for HO-Tyr/Arg"out" and black line for ⁻O-Tyr/Arg"out".

4.6 as described recently[1] and soaked in buffers with varying pH values. X-ray structures of *Mag*KatG2 at pH 3, 5.5, and 7.0 were obtained at 1.4, 1.4, and 1.7 Å resolution (Figure 1 and Table 1).

Comparative analyses show that the overall structure remains unchanged at these pH values with respect to the first reported *Mag*KatG2 structure (1.55 Å, PDB entry 3UT2)[1] with two exceptions, namely the modification on the indole nitrogen of the adduct tryptophan (Trp140) and the conformation(s) of the flipping arginine (Arg461). Also, the electronic density maps show some extra density 15 Å from the first traced residue (Thr50) of one of the subunits, which could account for some of the missing residues of this flexible N-terminus.

The indole nitrogen from Trp140 is not modified in any of the structures analyzed in this work, whereas it was modified with a peroxide group in the first *Mag*KatG2 structure and also in many of the reported *Bp*KatG and *Mt*KatG structures. This suggests that formation of this modification seems to be affected by subtle changes in the environmental conditions. The conformation of Arg461 changes from fully "out" to fully "in" between pH 3 and 7 (Figure 1 and Table 1). Consistently, at pH 5.5, the side chain of Arg461 shows a poor electron density suggesting mixed "in" and "out" conformations, though in the first *Mag*KatG structure (at pH 4.6), Arg461 showed ∼100% "in" conformation. The mobility of Arg461 at pH 5.5 is additionally underlined by the fact that the electron density for the "out" conformation is split (Figure 1).

The "in" conformation of Arg461 exhibits a hydrogen bond between one of the nitrogens of its guanidinium group and the tyrosinate oxygen of the MYW adduct (Figure 1). In the "out" conformation, Arg461 is making a hydrogen bond with the amide oxygen of Gln625 close to a conserved region that includes three arginines (Arg528, Arg533, and Arg540) (Figure 2 and Supplemental Figure 2). These observations confirm the conformational versatility of Arg461 in *Mag*KatG2 with a pH dependency that appears to be shifted with respect to prokaryotic KatGs.

Molecular dynamics simulation underlines the existence of H-bonds between the guanidinium nitrogens of Arg461 in the "out" conformation and the amide oxygen of Gln625 (32 and 36% occurrence in the 50 ns simulation) (Figure 2). In the known X-ray structures of prokaryotic KatGs, the corresponding residue is a serine (Ser590 in *Bp*KatG or Ser583 in *Mt*KatG and Ser564 in *Se*KatG1) and Arg in its "out" conformation comes closest to the oxygen of its side chain at distances of ∼3.5 Å (Supplemental Figure 2).[32] Additionally, in its "out" conformation, the backbone oxygen of Arg461 is H-bonded to the guanidinium group of Arg533 (30, 18, and 39% occurrence) (Figure 2). This residue is also found in prokaryotic KatGs (Supplemental Figure 2). Split electron density for the side chain of Arg533 in crystal structures as well as MD simulations suggests increased flexibility of its side chain (see below). In any case, the N-terminal domain of *Mag*KatG2 ends with Pro475, clearly demonstrating that mobile Arg461 in the "out" conformation interacts solely with residues from the C-terminal domain (Figure 2) that forms an accessible cavity for this flexible basic amino acid.

In summary, the crystal structures of *Mag*KatG2 underline the mobility of Arg461 and demonstrate that, in contrast to prokaryotic KatGs, the "in" conformation is also found in crystal states under more acidic conditions. This correlates with the more acidic pH optimum of the *catalatic* activity (i.e., pH 5.25) of *Mag*KatG2 compared to that of prokaryotic KatGs (see below).

Molecular Dynamics Simulations. Next, we explored the role of the protonation state of adduct Tyr273. The starting *Mag*KatG2 coordinates used in the MD simulations were derived from the high-resolution (1.55 Å) structure (PDB entry 3UT2).[1] Although *Mag*KatG2 is a homodimer, the protomers (each being composed of an N-terminal heme-containing domain and a C-terminal domain) work independently. Thus, for the sake of computational convenience, models were constructed with only one protomer, half of the *Mag*KatG2 molecule.

DOI: 10.1021/acs.biochem.6b00436
Biochemistry 2016, 55, 3528−3541

Four 50 ns MD simulations were performed with four different starting situations with Tyr273 either protonated (HO-Tyr273) or deprotonated ($^{-}$O-Tyr273) and Arg461 in the "in" or "out" conformation: HO-Tyr/Arg"out", HO-Tyr/Arg"in", $^{-}$O-Tyr/Arg"out", and $^{-}$O-Tyr/Arg"in". Within 50 ns, changes in the orientation of the Arg461 side chain were seen only in the $^{-}$O-Tyr/Arg"out" model (Figure 2). During this simulation, the side chain of Arg461 rotates from the "out" conformation to the "in" conformation. In the final (50 ns) structure, the side chain is slightly displaced with respect to the experimental crystallography data, so that the distance between the guanidinium group and the tyrosinate oxygen is significantly longer (5.4 ± 0.3 Å), suggesting the existence of a bridging water molecule (Figure 2). Furthermore, it was noticed that the side chain of Arg533 might move away from Arg461 when the latter is in the "in" conformation.

Next, we calculated the differences in the free energy (ΔG) for Arg461 among four 10 ns MD simulations of the starting models HO-Tyr/Arg"out", HO-Tyr/Arg"in", $^{-}$O-Tyr/Arg"out", and $^{-}$O-Tyr/Arg"in". Figure 3 compares the four hypothetical processes, clearly demonstrating the favorable interaction between Arg461 and the adduct Tyr273 in its deprotonated state. Protonation of Tyr273 forces Arg461 to adopt the "out" conformation. Because in the crystal state the "in" conformation was even present at pH 4.6 (see above), this might suggest a very low pK_a value for the side chain of Tyr273 in *Mag*KatG2.

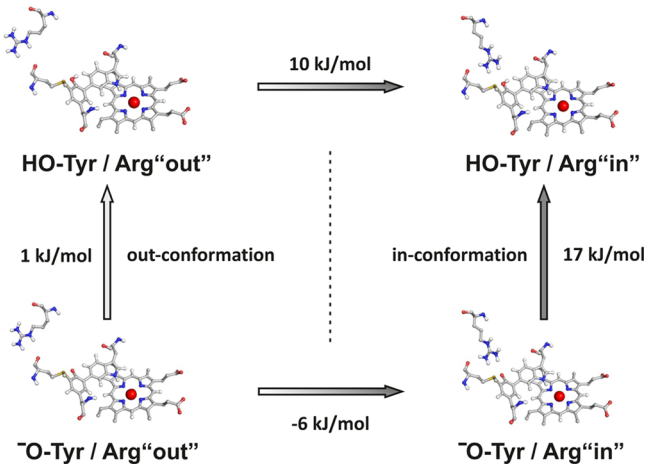

Figure 3. Free energy differences (ΔG) of Arg461 among four independent 10 ns molecular dynamics simulations. The evaluated models were HO-Tyr/Arg"out", HO-Tyr/Arg"in", $^{-}$O-Tyr/Arg"out", and $^{-}$O-Tyr/Arg"in". For calculation of the free energies for the four hypothetical processes, see Materials and Methods.

Spectral Features, Enzymatic Activities, and Thermal Stabilities of Wild-Type *Mag*KatG2 and the Mutant Arg461Ala. The UV−vis spectrum of recombinant dimeric *Mag*KatG2 (monomer size of 85 kDa) at pH 7.0 has been published recently.[2] At room temperature, the high-spin ferric protein shows a Soret maximum at 404 nm, Q-bands at 505 and 539 nm, and a broad CT1 band at 640 nm. Figure 4B demonstrates that these spectral signatures are very similar in the pH range of 4.5−8.5, suggesting unchanged heme cavity architecture. This is reflected by almost identical coordinates of residues in the vicinity of the prosthetic group as seen in the X-ray structures. Upon exchange of Arg461 with Ala, the absorbance maximum of the mutant was only slightly red-shifted but still reflects the presence of high-spin ferric protein (Figure 4A), suggesting very similar active site geometries of wild-type and mutant protein. Identical UV−vis spectra of Arg461Ala were obtained between pH 4.5 and 8.5 with a Soret maximum at 406 nm, Q-bands at 506 and 541 nm, and a broad CT1 band at 642 nm.

Figure 5 shows that elimination of the mobile arginine significantly modifies the catalase activity. In contrast to the wild-type enzyme that shows a maximal activity at pH 5.25 (k_{cat} = 6450 s^{-1}), the variant Arg461Ala exhibits a significantly lower specific activity and shows a plateau between pH 4.5 and 7.5 (Figure 5A). At pH 5.5, the corresponding k_{cat} value was determined to be 270 s^{-1}, which is 24 times smaller than that of the wild-type protein at its pH optimum. In prokaryotic KatGs, the impact of exchange of mobile Arg with Ala was very similar (20−26-fold decrease in k_{cat} at the pH optimum),[14,33] but the catalase activity of Arg461Ala is still more than 2 orders of magnitude higher than that of conventional (monofunctional) peroxidases[31] or KatGs with a disrupted Met-Tyr-Trp adduct.[14,17−19,23−27] Interestingly, the specific catalase activity of the mutant increases with a decrease in pH from 4.5 to 3.0 (see the inset of Figure 5A), but it is important to note that in this very acidic pH range H_2O_2 degradation was incomplete, suggesting inactivation of the enzyme.

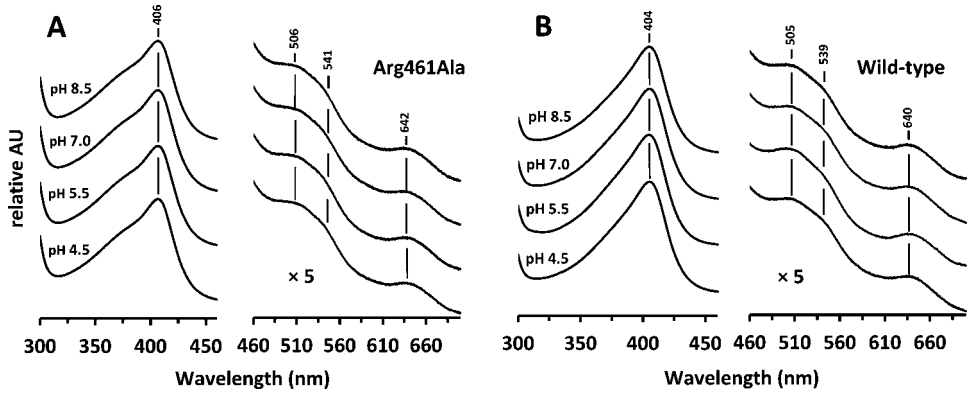

Figure 4. UV−vis spectra of wild-type *Mag*KatG2 and the Arg461Ala variant at pH 4.5−8.5. Conditions: 7 μM protein in either 50 mM citrate-phosphate buffer (pH 4.5 and 5.5) or 50 mM phosphate buffer (pH 7.0 and 8.5). The wavelength range of 460−700 nm is expanded by a factor of 5 for the sake of better visibility.

DOI: 10.1021/acs.biochem.6b00436
Biochemistry 2016, 55, 3528−3541

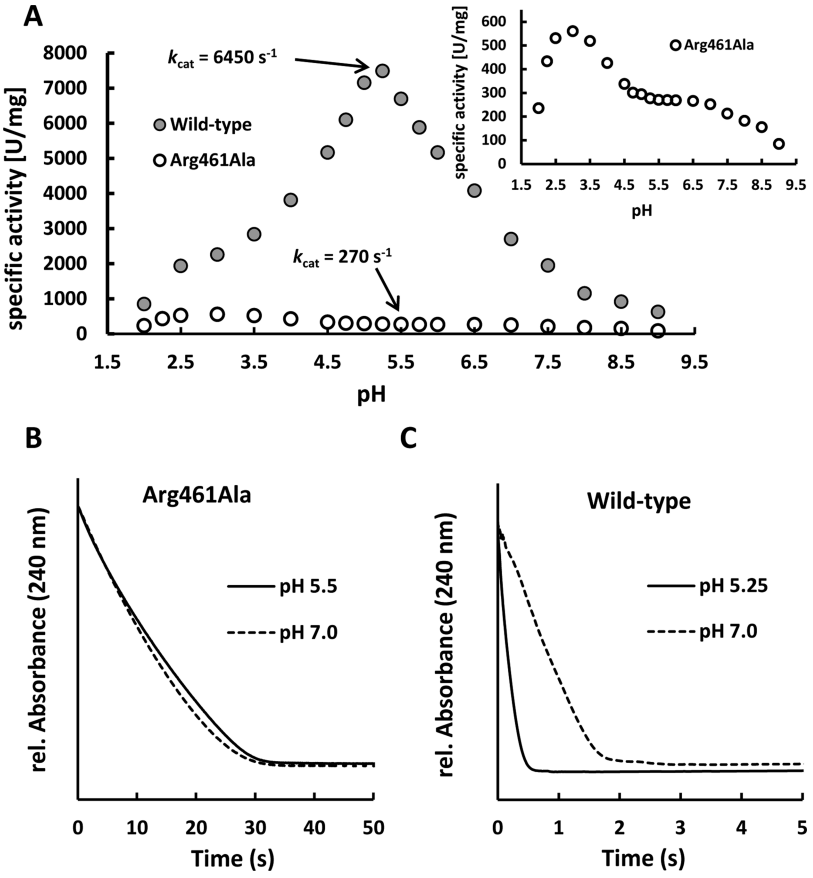

Figure 5. pH dependence of catalase activity of wild-type *Mag*KatG2 and the variant Arg461Ala. (A) Polarographically determined specific activity plotted vs pH. At the pH optimum of wild-type *Mag*KatG2, k_{cat} = 6450 s^{-1}, which compares with a value of 270 s^{-1} at the plateau at pH 5.5 for Arg461Ala. (B) Kinetics of H_2O_2 degradation (10 mM) by 2 μM Arg461Ala followed at 240 nm at pH 7 and 5.5. For comparison, panel C shows the kinetics of degradation of 10 mM H_2O_2 mediated by 2 μM wild-type enzyme at pH 7.0 and 5.25.

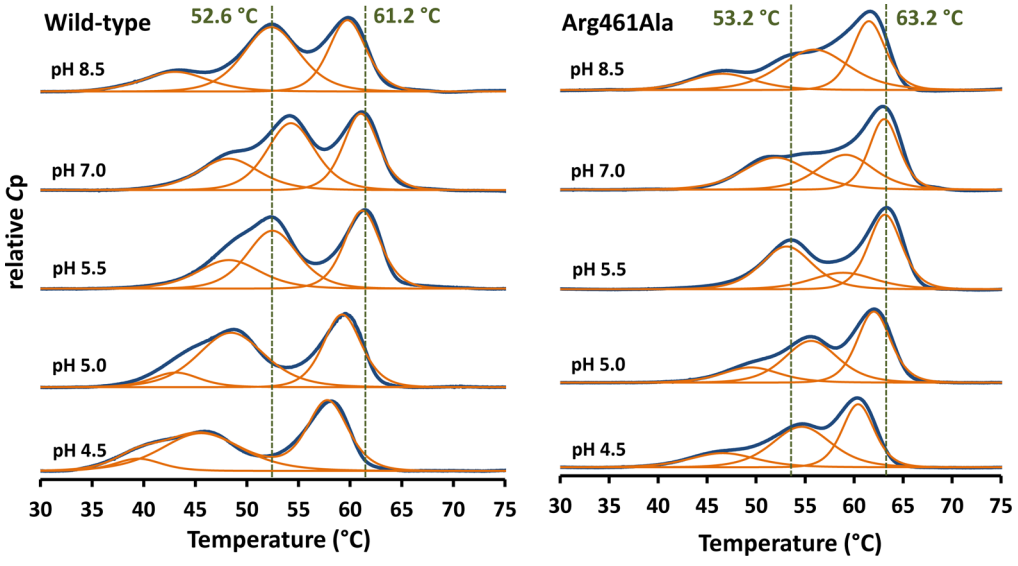

Figure 6. pH dependence of the thermal stability of wild-type *Mag*KatG2 and the variant Arg461Ala. Differential scanning calorimetric measurements were performed with 5 μM protein in either 50 mM citrate-phosphate buffer (pH 4.5−5.5) or 50 mM phosphate buffer (pH 7.0 and 8.5) using a heat rate of 60 °C h^{-1}. The obtained baseline-corrected thermograms are shown as bold blue lines, and the corresponding fitted non-two-state transition peaks are depicted as thin orange lines. Dashed vertical lines have been inserted for the presentation of respective melting temperatures.

These polarographically determined data are fully confirmed by following the degradation of hydrogen peroxide spectrophotometrically at 240 nm in the stopped-flow apparatus. Figure 5B shows two representative time traces for the degradation of 10 mM H_2O_2 by 2 μM Arg461Ala at pH 5.5 and 7.0. It is clearly shown that (i) there is no pH dependence

DOI: 10.1021/acs.biochem.6b00436
Biochemistry 2016, 55, 3528−3541

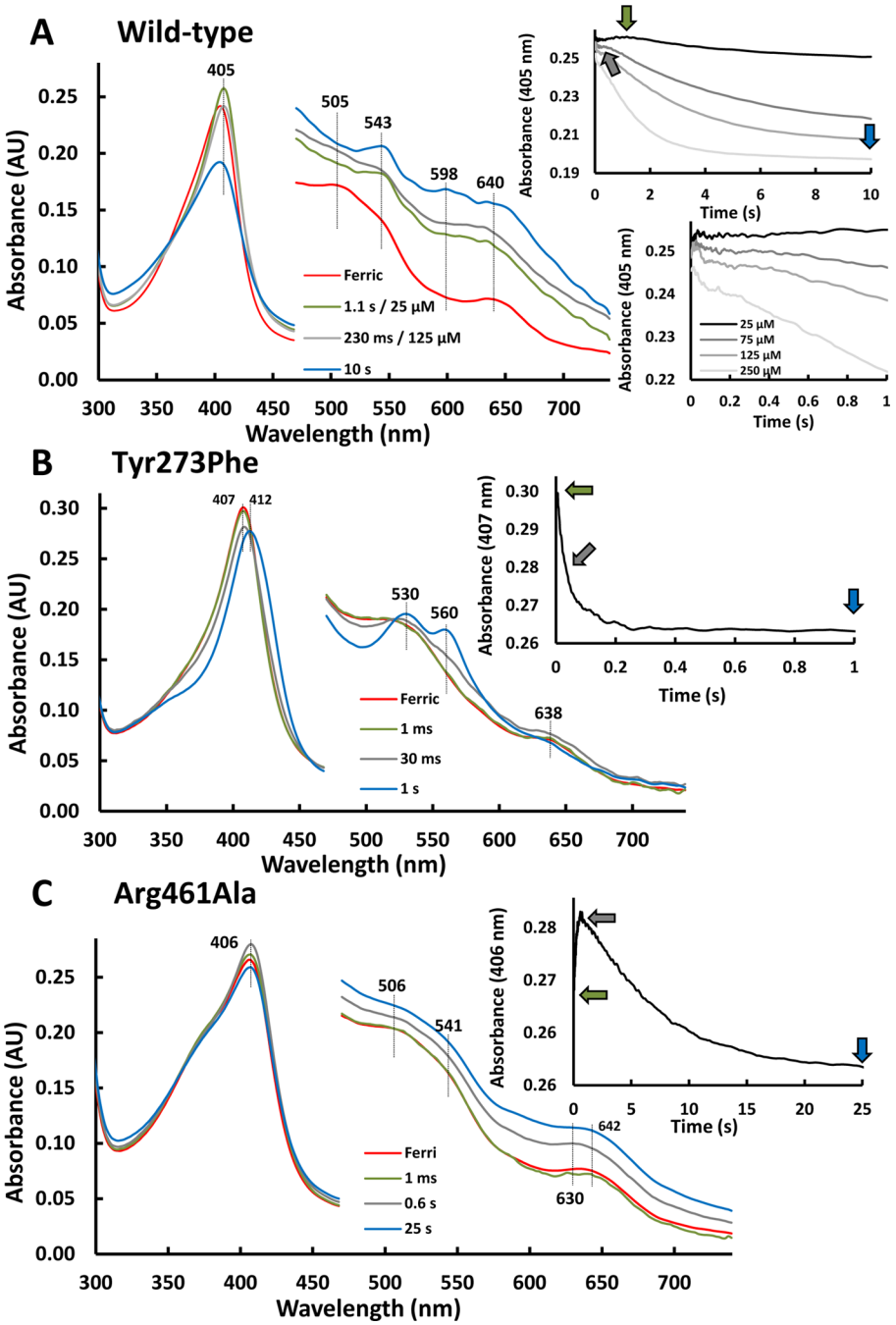

Figure 7. Reaction of ferric wild-type *Mag*KatG2 and the variants Tyr273Phe and Arg461Ala with peroxyacetic acid at pH 7.0. Red lines indicate the ferric resting state and green lines the intermediate present immediately after mixing. Data for intermediate species formed at later time points are colored gray and blue. Typical time traces recorded at the Soret maximum are shown. Arrows indicate the time points of selection of the spectra. (A) Reaction between 2.5 μM wild-type *Mag*KatG2 in 50 mM phosphate buffer (pH 7.0) and 25, 75, 125, or 250 μM peroxyacetic acid. (B) Reaction between 3 μM Tyr273Phe variant in 50 mM phosphate buffer (pH 7.0) and 3 μM peroxyacetic acid. (C) Reaction between 2.7 μM Arg461Ala variant in 50 mM phosphate buffer (pH 7.0) and 25 μM peroxyacetic acid.

and (ii) the mutant is able to fully degrade H_2O_2 (10 mM H_2O_2 corresponds to $\Delta Abs_{240} \sim 0.4$) without being inhibited ([substrate]/[enzyme] = 5000). For comparison, Figure 5C shows the degradation of 10 mM H_2O_2 by the wild-type enzyme at pH 5.25 and 7.0. Both panels demonstrate the higher *catalatic* activity as well as the pH dependence of the wild-type enzyme.

In contrast to the *catalatic* activity, the peroxidase activity is slightly enhanced upon exchange of Arg461 with Ala in a manner independent of whether peroxoacetic acid or H_2O_2 is used for initiation of reaction (Supplemental Figure 3). With guaiacol as the one-electron donor, wild-type *Mag*KatG2 shows a pH optimum around pH 7.0 with both peroxides, whereas oxidation of guaiacol by Arg461Ala with H_2O_2 shows a broad optimum around pH 6.5 and with PAA a plateau between pH 5.5 and 6.5.

Next, we were interested in the impact of mobile Arg461 on the thermal stability of *Mag*KatG2. At room temperature, both wild-type *Mag*KatG2 and the variant Arg461Ala are dimeric in solution and show a single band at 85 kDa in sodium dodecyl

DOI: 10.1021/acs.biochem.6b00436
Biochemistry 2016, 55, 3528−3541

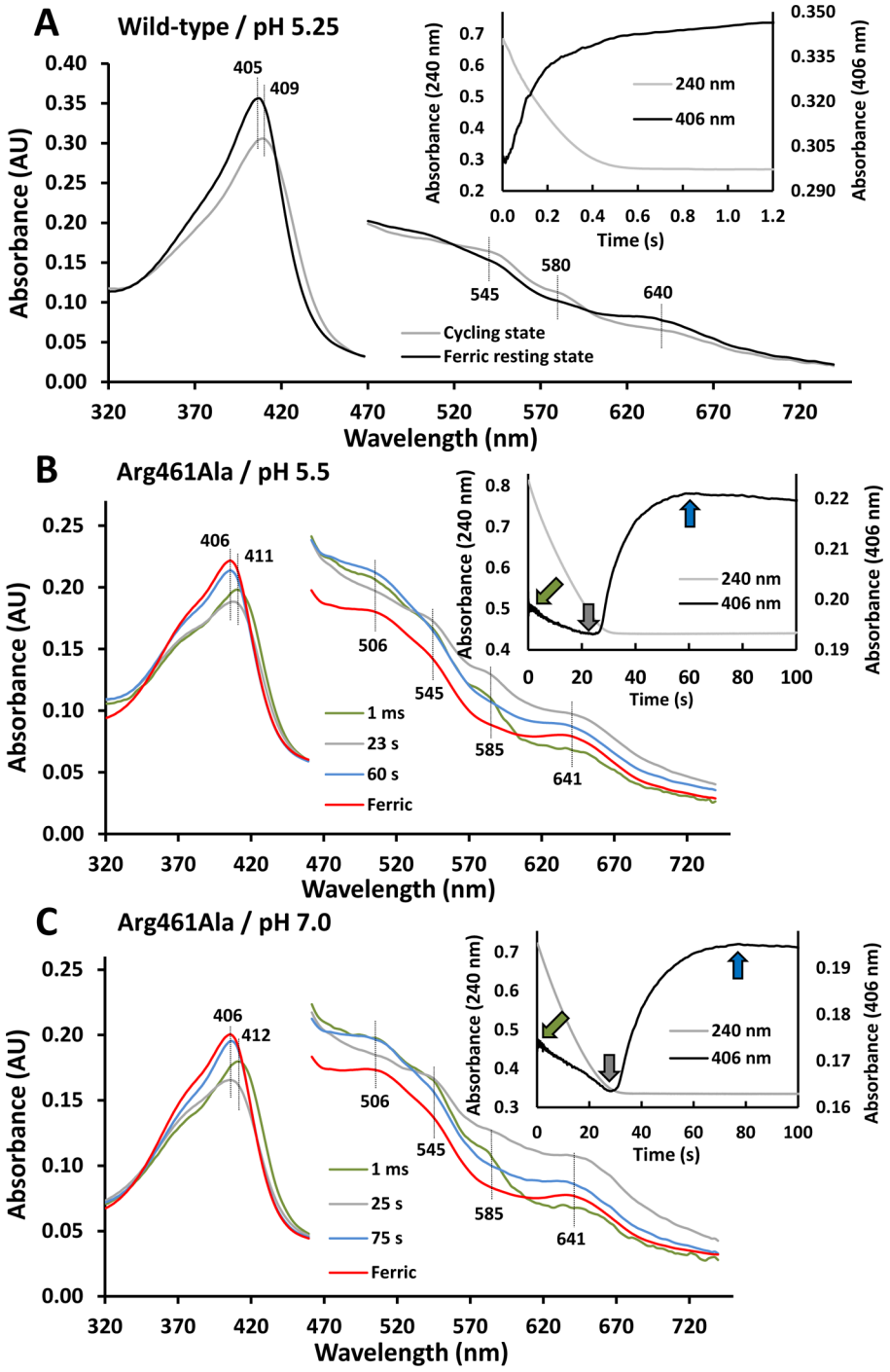

Figure 8. Reaction of ferric wild-type *Mag*KatG2 and the Arg461Ala variant with hydrogen peroxide. (A) Wild-type *Mag*KatG2 reacting with 10 mM hydrogen peroxide. The black line is for the ferric protein, and the gray spectrum represents spectral signatures of the dominating intermediate during H_2O_2 degradation. The inset depicts the corresponding single traces at 240 nm (decay of hydrogen peroxide) and 406 nm (Soret maximum of ferric protein). (B and C) Reaction of the variant Arg461Ala with 10 mM hydrogen peroxide at pH 5.5 and 7.0, respectively. Red lines show data for the ferric resting state and green lines data for the intermediate formed directly after mixing. Data for species formed at later time points are colored gray and blue. Insets show the corresponding time traces at 240 and 406 nm. For better visualization, important absorbance maxima have been marked and labeled. Final conditions: (A) 3.6 μM wild-type protein in 50 mM phosphate-citrate buffer (pH 5.25), (B) 2.0 μM Arg461Ala in 50 mM phosphate-citrate buffer (pH 5.5), and (C) 2.0 μM Arg461Ala in 50 mM phosphate buffer (pH 7.0).

sulfate−polyacrylamide gel electrophoresis under reducing conditions (not shown). Under nonreducing conditions, one band at 170 kDa is observed for both proteins, suggesting that the *Mag*KatG2-typical interchain disulfide bridges[1] between Cys55 and Cys74 of the N-terminal domains are intact in both enzymes. The far-UV circular dichroism (CD) spectra at pH 7.0 of both proteins are identical (insets of Supplemental Figure 4), suggesting that elimination of Arg461 has no impact on the overall secondary structure composition of the protein.

Figure 6 compares the temperature-mediated unfolding pathways of wild-type *Mag*KatG2 and the mutant Arg461Ala between pH 4.5 and 8.5 followed by differential scanning

DOI: 10.1021/acs.biochem.6b00436
Biochemistry 2016, 55, 3528−3541

calorimetry (DSC). It has to be mentioned that at pH ≤4.0 both proteins started to precipitate with an increase in temperature. At the pH optimum of *catalatic* activity of the wild-type enzyme, unfolding of both proteins follows a two-state unfolding pathway with two main and well-separated transitions. The mutant protein has a slightly higher thermal stability (T_m values at 53.2 and 63.2 °C) compared to that of the wild-type protein (52.6 and 61.2 °C). Thermal unfolding followed by CD spectroscopy at 208 nm (typical minimum in ellipticity of α-helices) and at the Soret minimum of 395 nm (Supplemental Figure 4) clearly demonstrates that the N-terminal heme-containing and cross-linked domain in *Mag*KatG2 is much more stable than the C-terminal domain. Loss of heme ellipticity occurs between 60 and 66 °C. In prokaryotic KatGs, the N-terminal domain has a much lower thermal stability and both endotherms merge.[42]

The thermal stability of the N-terminal domain of both wild-type *Mag*KatG2 and the variant Arg461Ala is highest between pH 5.5 and 7.0 and slightly decreases under more acidic and basic conditions. The symmetric shapes of the endotherms clearly suggest cooperative unfolding of the heme-containing domain at all investigated pH values. By contrast, the C-terminal domain seems to be much more susceptible to denaturation. Apart from pH 5.5, unfolding of the C-terminal domain becomes uncooperatively reflected by a broad peak tailing, which is more pronounced in wild-type *Mag*KatG2 (Figure 6). The DSC data suggest that at pH 4.5 the C-terminal domain of wild-type *Mag*KatG2 starts to unfold already at 35 °C.

Transient-State Kinetics of Ligand Binding and Reaction with Peroxides. Manipulation of the mobile Arg461 does not influence the binding kinetics of the low-spin ligand cyanide, again reflecting identical heme cavity architecture and accessibility. At pH 7.0, the binding rates and calculated K_D values are $(5.4 \pm 0.2) \times 10^5$ M^{-1} s^{-1} and 14.4 μM (wild-type) and $(3.5 \pm 0.3) \times 10^5$ M^{-1} s^{-1} and 10.2 μM (Arg461Ala), respectively (Supplemental Figure 5).

Figure 7 shows the changes in the electronic absorption spectra of wild-type *Mag*KatG2 and the variants Tyr273Phe and Arg461Ala upon reaction of the respective ferric proteins with peroxyacetic acid (PAA) at pH 7.0. The mutant Tyr273Phe was included in this study, because it represents the monofunctional variant without the Met-Tyr-Trp adduct and thus without *catalatic* activity. The reaction of Tyr273Phe with equimolar PAA leads to formation of a Compound II-like spectrum with bands at 412, 530, and 560 nm within 0.5 s, which most probably represents a Compound I* resulting from internal electron transfer from remote aromatic amino acids to transiently formed Compound I (Figure 7B). Both the spectral signatures and the kinetics of interconversion were almost identical at pH 5.5.

When wild-type *Mag*KatG2 or the mutant Arg461Ala was mixed, completely different spectral transitions were monitored compared to those of Tyr273Phe, clearly suggesting participation of the KatG-typical adduct in the redox reactions. Several distinct phases could be observed. In wild-type *Mag*KatG2, an increase in intensity and a narrowing of the Soret band were observed, followed by a "lag phase" and, finally, by a decrease in the Soret absorbance maximum at 405 nm, leading to an intermediate with absorbance bands at 407, 543, 598, and 640 nm. The latter conversion follows an apparent bimolecular rate constant of 7.5×10^3 M^{-1} s^{-1} at pH 7.0 (and 6.7×10^3 M^{-1} s^{-1} at pH 5.0) but might represent a steady-state shift to classical Compound I (blue spectrum in Figure 7A). The length of the lag phase decreased with an increase in PAA concentration (see insets of Figure 7A). Both the spectral signatures and the kinetics of interconversion were similar at pH 5.5 (not shown).

The kinetics of absorbance changes of the mutant Arg461Ala mixed with PAA also showed an initial increase at Soret absorbance followed by a decrease in Soret intensity (inset of Figure 7C). In contrast to the case for wild-type *Mag*KatG2, the lag phase and the hypochromicity of the Soret absorbance of the resulting intermediate were less pronounced (Figure 7C). Similar kinetic and spectral transitions were observed at pH 5.5.

Next, we elucidated the spectral signatures of the redox intermediate of *Mag*KatG2 that dominates during H_2O_2 degradation (Figure 8). Upon reaction of 3.6 μM wild-type ferric protein with 10 mM H_2O_2 at pH 5.25 within 1 ms, a low-spin species was formed showing a slighly red-shifted Soret band, two peaks at 545 and 580 nm in the Q-band region, and disappearance of the high-spin CT band at 640 nm. This spectrum resembles that of Compound III, which is observed when monofunctional peroxidases (e.g., APx) are mixed with millimolar H_2O_2.[31] With *Mag*KatG2, the reaction is very fast, and within 500 ms, 10 mM H_2O_2 is fully degraded and the ferric enzyme state is restored (inset of Figure 8A). These observed kinetics and spectral transitions during reaction of the eukaryotic wild-type catalase-peroxidase with hydrogen peroxide are reminiscent of the corresponding reactions found in prokaryotic KatGs below pH 7.0 as first described by Jakopitsch et al.[23] With both prokaryotic and eukaryotic KatGs, in the alkaline pH region (pH >7.0), the spectral features of the dominating redox intermediate during H_2O_2 degradation are different. Together with a red-shifted Soret peak, a broad shoulder around 520 nm and loss of the high-spin CT band are typically observed immediately after mixing with hydrogen peroxide.[2,23]

Both the kinetics of degradation of hydrogen peroxide and the accompanying spectral transitions of the variant Arg461Ala with hydrogen peroxide revealed significant differences compared to those of the wild-type enzyme. Panels B (pH 5.5) and C (pH 7.0) of Figure 8 show the corresponding reactions between 2 μM Arg461Ala and 10 mM H_2O_2. Similar to that of the wild-type protein, the first monitored spectrum immediately after mixing in the stopped-flow apparatus shows a red-shifted Soret band and spectral features in the visible region that are reminiscent of the species seen in the wild-type protein at pH 5.25, i.e., peaks at 545 and 585 nm (green spectra in panels B and C of Figure 8). In contrast to the wild-type protein, 1 ms after mixing the mutant protein still shows some spectral features of the ferric state, reflecting its slower reactivity toward H_2O_2.

An important difference between wild-type and mutant protein concerns the dominating redox intermediate during H_2O_2 degradation. In wild-type *Mag*KatG2, the intermediate immediately seen after mixing with H_2O_2 is fully present and visible during H_2O_2 degradation until (after complete peroxide depletion) the ferric spectrum is recovered. In case of the mutant protein, a steady-state shift to a mixture of species including Compound I (as seen in the reaction with peroxoacetic acid) is observed at both pH values (gray spectra in panels B and C of Figure 8), until (after complete peroxide depletion) the resting state is re-formed. Restoration of the ferric state after H_2O_2 depletion is slightly faster at pH 5.5 than at pH 7.0 (compare insets of panels B and C of Figure 8). Very

DOI: 10.1021/acs.biochem.6b00436
Biochemistry 2016, 55, 3528−3541

similar spectral transitions are also seen at pH 3 and 8.5 (not shown). Thus, the dominating redox intermediate of Arg461Ala at alkaline pH still exhibits Compound III-like spectral features, which is in contrast to wild-type *Mag*KatG2 and the prokaryotic counterparts (see above).

DISCUSSION

Heme peroxidases like cytochrome *c* peroxidases (C*c*P) or ascorbate peroxidases (APx) are known to be irreversibly inhibited by excess hydrogen peroxide in the absence of exogenous one-electron donors.[31] Despite the fact that the core of the catalytic domain of bifunctional KatG bears a strong resemblance to C*c*P and APx,[11] catalase-peroxidases are able to efficiently dismutate hydrogen peroxide without being inhibited. Moreover, in KatG, the catalase activity clearly dominates over the peroxidase activity and even rivals the activity of monofunctional catalases.[9,10] In the past decade, the structural peculiarities like KatG-typical insertions (loops) and the presence of an autocatalytically and posttranslationally formed redox-active Met-Tyr-Trp adduct close to heme *b* have been analyzed in detail and brought into context with the mechanism of H_2O_2 dismutation (see recent reviews[43,44]). However, there is still an ongoing debate about the exact mechanism of the H_2O_2 oxidation reaction.[43,44]

So far, almost all experimental and computational data are derived from work on prokaryotic KatGs. The recent discovery of eukaryotic KatGs[1,2,12,35,36] now opens the possibility of querying postulated mechanisms and/or specifying so far unsolved mechanistic details. The selected model enzyme *Mag*KatG2 has conformational and thermal stability much higher than those of the prokaryotic counterparts and, interestingly, has a pH optimum of catalase activity at pH 5.25 compared to the range of pH 6.0−6.5 reported for prokaryotic KatGs.[43,44]

In this work, we have focused on the perhaps most intriguing modulator of catalase activity of KatG, i.e., the mobile arginine that is fully conserved in both prokaryotic and eukaryotic KatGs.[35,36] Data from prokaryotic KatGs and this work clearly show that it is integral to the catalase activity because substitution with anything but Lys greatly diminishes the catalase but not the peroxidase activity.[14,32−34] Similar to the case in prokaryotic KatGs, Arg461 in *Mag*KatG2 is mobile as demonstrated by X-ray crystallography and MD simulations; however, in contrast to prokaryotic KatGs, the "in" conformation (i.e., ionic interaction with adduct Tyr273) is present also at acidic pH values as seen in the original structure at pH 4.6[2] and the novel structure obtained from soaking at pH 5.5. Only at a very acidic pH, the "out" conformation dominates (Figure 1). In the "out" conformation, Arg461 interacts exclusively with residues from the C-terminal (catalytically inactive) domain. In *Mag*KatG2, Arg461 in its "out" conformation is hydrogen bonded with the amide oxygen of Gln625, whereas in *Bp*KatG, *Mt*KatG, and KatG from *Synechococcus elongatus*, it is H-bonded with the side chain of a serine. In this context, it is important to note that the C-terminal domain in *Mag*KatG2 has a low conformational and thermal stability at pH ≤4.5 in contrast to the N-terminal domain (Figure 6). It is well-known that an intact heme cavity architecture of KatG depends to some extent on the gene-duplicated C-terminal domain. KatG lacking this domain or parts of it displays exclusively low-spin heme and loses both the catalase and peroxidase activity.[20,45] Considering the very low stability of the C-terminal domain in the acidic pH region, it is reasonable to assume that the binding site of Arg461 in the "out" conformation collapses in solution at very low pH values (despite the fact that it was still intact in the crystal soaked with buffer at pH 3.0). This suggests that enzyme activity data obtained from measurements at pH <4.0 might be problematic.

In any case, we could demonstrate that the "in" conformation of Arg461 dominates in the crystal structures of *Mag*KatG2 at pH ≥4.5. Additionally, the performed 50 ns MD simulations and calculations of differences in the free energy among four MD simulations of various starting models clearly show that Arg461 is mobile and that deprotonation of Tyr273 thermodynamically favors the "in" conformation, whereas its protonation promotes Arg461 to adopt the "out" position. These data might suggest that the pK_a of Tyr273 is lower compared to those of prokaryotic KatGs, but it is also important to keep in mind that the position of the mobile arginine itself modulates the pK_a of the adduct tyrosine. As shown in this paper, the mobile arginine in the "out" position has different interaction partners in prokaryotic and eukaryotic KatGs, and it is tempting to speculate whether these differences favor a stronger tendency in *Mag*KatG2 to adopt the "in" conformation and give rise to a lower pK_a. Additionally, it is important to note that the adduct is oxidized during enzyme turnover (reflected in the intermediate states Compound I* and Compound III*), which in addition promotes formation of tyrosinate and ionic interaction with Arg461 (see below).

Similar to the case for prokaryotic KatGs, elimination of Arg461 by mutation to Ala partially impairs the catalase activity. Additionally, the pH dependence is modified, and similar *catalatic* activity is observed between pH 4.5 and 7.5. The turnover number of Arg461Ala at pH 5.5 is only 4% of the k_{cat} of the wild-type enzyme at its pH optimum. By contrast, the peroxidase activity is almost unaffected by elimination of Arg461. This clearly underlines the fact that for conventional peroxidase activity neither an intact adduct[2,16−19] nor the presence of the mobile arginine is needed, but both fully conserved structural KatG-typical features are essential for efficient oxidation of hydrogen peroxide.

Similar to the case for cytochrome *c* peroxidase, the characteristic green porphyrin π cation radical Compound I (typical for horseradish peroxidase or ascorbate peroxidase)[46] does not accumulate in KatG when it is mixed with H_2O_2. In C*c*P, Compound I* carries the proximal Trp191$^{\bullet+}$ radical.[46] In KatG, transiently formed Compound I (reaction I) is also rapidly converted to Compound I* (reaction II) as demonstrated by UV−vis stopped-flow spectroscopic studies[23,24] and freeze-quench EPR.[14,24] Studies of KatG from *Mycobacterium tuberculosis* (*Mt*KatG) demonstrated that the Met-Tyr-Trp adduct radical[14,24] is formed immediately after mixing with H_2O_2 and persists during the time interval corresponding to the H_2O_2 consumption kinetics. Importantly, the spin concentration could not be increased at higher H_2O_2 concentrations,[14] and deletion of the mobile arginine had no impact on reaction II; i.e., the corresponding mutant produces a similar yield of adduct radical, and the persistence of the radical signals coincided with the period required for H_2O_2 consumption.[14]

Formation of Compound I* should be independent of the oxidant used for the two-electron oxidation of the ferric resting state. The effects of the produced acid notwithstanding, the chemistry of the peroxide (PAA vs H_2O_2) determines the kinetics of reaction I but has no direct impact on the internal electron transfer represented by reaction II. It was interesting to

DOI: 10.1021/acs.biochem.6b00436
Biochemistry 2016, 55, 3528−3541

see that, with both the wild-type protein and the mutant Arg461Ala, the reaction with peroxacetic acid was biphasic, reflected by an increase in absorbance followed by hypochromicity at the Soret maximum (Figure 7A,C). A similar kinetics is also seen in prokaryotic KatGs, and the increase was interpreted as formation of a complex between the respective ferric proteins and PAA.[47,48] However, in the absence of the covalent adduct (e.g., in Tyr273Phe) but with the distal tryptophan in place (as in *Cc*P and APx)[2,49] and identical substrate channel architecture, the PAA-mediated reaction was always accompanied by a monophasic decrease in Soret absorbance only. Thus, one might speculate that the first fast phase of the reaction of ferric wild-type *Mag*KatG2 or Arg461Ala with PAA reflects the rate-limiting step in Compound I* formation that is followed by a steady-state shift to conventional Compound I. Because H_2O_2 is absent, Compound I* is relatively stable and can be reduced to the resting state only by electron transfer from the protein matrix that becomes oxidatively damaged.[48] As a consequence, reaction II becomes more and more impaired and (classical) Compound I accumulates with time. In contrast to the H_2O_2-mediated conversion, the adduct radical has a significantly longer life span in the KatG/PAA system.

Elimination of the mobile arginine has no impact on the H_2O_2-mediated oxidation of the enzyme to Compound I* (reactions I and II) or formation of Compound III* (reaction III), but it impairs the effective adduct radical utilization in the second half-reaction, i.e., the release of O_2 (reaction IV). Stopped-flow kinetic investigations of both prokaryotic and eukaryotic KatGs mixed with an excess of H_2O_2 around the pH optimum and in the acidic pH region typically show the immediate (<1 ms) formation of an intermediate with a red-shifted Soret band and two typical bands at 542−545 and 580−585 nm[2,14,19,23,24] that strongly resemble the spectral signatures of Compound III (oxyheme species) of peroxidases, including *Cc*P[50] and APx,[51] or KatG variants with a disrupted adduct.[2,14,19] In contrast to monofunctional peroxidases[51] in KatG, (i) oxidation of H_2O_2 according to reaction III is several orders of magnitude faster[52] and (ii) oxyheme formation occurs in the presence of the adduct radical thus denoted Compound III*.[14,24] The fact that carbon monoxide (which binds to only ferrous heme as found in Compound III*) interferes with the catalase reaction of KatG (but not with monofunctional catalases) under both acidic and basic conditions[14] suggests that Compound III* formation occurs throughout the pH range of the catalase reaction. As a conclusion, we propose that elimination of the KatG-typical arginine has no impact on reactions I−III and thus Compound III* formation as shown for both *Mt*KatG[14] and *Mag*KatG2 (Figure 8).

The question remains about the role of Arg461 in reaction IV, i.e., the release of O_2? Importantly, significant differences between wild-type *Mag*KatG2 and the mutant Arg461Ala in the H_2O_2-mediated spectral conversions were observed. There was always a coincidence between H_2O_2 consumption and the persistence of the dominating low-spin intermediate in wild-type *Mag*KatG2. This was also observed with prokaryotic KatGs.[14,23] Moreover, for *Mt*KatG, it could be demonstrated that this coincidence included also the persistence of the adduct radical. In the absence of the mobile arginine upon addition of H_2O_2, the same redox intermediate is formed immediately after mixing but was then replaced in the time course of reaction by an intermediate with spectral signatures similar to that of (classical) Compound I (Figure 8B,C). It has been demonstrated by DFT calculations[14] that the ionic interaction between the side chain of the mobile arginine and the adduct Tyr favors the redox reaction between the adduct radical and the adjacent superoxide/dioxyheme of the Compound III* intermediate through electronic effects. In wild-type KatG, this effect will be favored at all pH values where the mobile arginine is in the "in" conformation. In the absence of the basic amino acid, the electron transfer between superoxide and the adduct radical is hampered, and consequently, the turnover of Compound III* is significantly retarded. Similar to the PAA-mediated reaction under this condition, the protein might act as a poor electron donor, thus providing a Met-Tyr-Trp adduct radical escape pathway. This is supported by the observation of pronounced formation of dityrosine cross-linked oligomers of KatGs that lack the mobile arginine.[14] This also suggests that the large amount of tryptophans and tyrosines found in the N-terminal domains of KatGs have an antioxidant role. In any case, as a consequence, (classical) Compound I accumulates during H_2O_2 degradation by Arg461Ala. This might also explain why in conventional (hand-mixing) EPR measurements an oxoiron(IV) porphyryl radical intermediate could be detected.[33]

In summary, in the case of *Mag*KatG2, the pH optimum of H_2O_2 dismutation was shown to be 5.25. Around the pH optimum and above, Arg461 is predominantly in the "in" conformation. Below pH 5.25, the catalase activity decreases most probably because Tyr273 is protonated and its interaction with Arg461 is disfavored and quenching of the adduct radical by the dioxyheme intermediate becomes slower. Additionally, the fact that the C-terminal domain starts to collapse below pH 4.5 must be taken into account, which additionally diminishes the *catalatic* activity. Above pH 5.25, the capability of *Mag*KatG2 to dismutate H_2O_2 decreases, too, despite the favorable interaction between Arg461 and Tyr273. At pH >7, the dominating redox intermediate during H_2O_2 degradation does not exhibit the Compound III-like spectral features[2,14,23] while the adduct radical is still present at normal abundance.[14] This might suggest that in wild-type *Mag*KatG2 at alkaline pH formation of Compound III* (reaction III) is slower than its turnover (reaction IV). As a consequence, Compound III* does not accumulate during turnover. It is known from monofunctional peroxidases that Compound III formation is pH-dependent and disfavored under alkaline conditions.[52] In contrast to the case for wild-type *Mag*KatG2, in the variant Arg461Ala Compound III* also accumulates at alkaline pH values, because in the mutant reaction IV is even slower than reaction III.

In conclusion, the role of the mobile Arg in *Mag*KatG2 and prokaryotic KatGs is to guarantee optimal electron transfer between the superoxide/dioxygen intermediate and the adduct radical. Its suppresses unspecific escape pathways of the adduct radical and oxidative damage of the protein. As a consequence, KatGs efficiently dismutate H_2O_2 and release O_2. Upon supporting the turnover of Compound III*, the mobile arginine helps to avoid both the release of superoxide and irreversible enzyme inhibition, which is typically observed when monofunctional peroxidases are incubated with H_2O_2 in the absence of one-electron donors.[31]

DOI: 10.1021/acs.biochem.6b00436
Biochemistry 2016, 55, 3528−3541

■ ASSOCIATED CONTENT

Supporting Information

The Supporting Information is available free of charge on the ACS Publications website at DOI: 10.1021/acs.biochem.6b00436.

Postulated mechanism of hydrogen peroxide dismutation mediated by catalase-peroxidase (Supplemental Figure 1), sequence alignment of 40 representative eukaryotic and prokaryotic catalase-peroxidase (KatG) sequences (Supplemental Figure 2), pH dependence of guaiacol oxidation by wild-type *Mag*KatG2 and the variant Arg461Ala (Supplemental Figure 3), temperature-mediated unfolding of the variant Arg461Ala followed by electronic circular dichroism spectroscopy (Supplemental Figure 4), and reaction of wild-type *Mag*KatG2 and the variant Arg461Ala with cyanide at pH 7.0 (Supplemental Figure 5) (PDF)

Accession Codes

Atomic coordinates and structure factors have been deposited in the Protein Data Bank as entries 5JHX, 5JHY, and 5JHZ.

■ AUTHOR INFORMATION

Corresponding Author

*Phone: +43-1-47654-6073. Fax: +43-1-47654-6059. E-mail: christian.obinger@boku.ac.at.

Funding

This project was supported by the Austrian Science Fund, FWF [Doctoral program BioToP-Biomolecular Technology of Proteins (W1224) and Projects P23855 and P25270] and the Vienna Science Technology Fund (LS08-QM03).

Notes

The authors declare no competing financial interest.

■ ABBREVIATIONS

KatG, catalase-peroxidase; *Mag*KatG2, secreted (extracellular) catalase-peroxidase from *M. grisea*; *Bp*KatG, KatG from *Burkholderia pseudomallei*; *Mt*KatG, KatG from *My. tuberculosis*; *Se*KatG, KatG from *S. elongatus*; *Syn*KatG, KatG from *Synechocystis* PCC6803; MYW, Met-Tyr-Trp, i.e., KatG-specific adduct; C*c*P, cytochrome *c* peroxidase; APx, ascorbate peroxidase; PAA, peroxyacetic acid; CD, circular dichroism; DSC, differential scanning calorimetry; EPR, electron paramagnetic resonance; MD, molecular dynamics; DFT, density functional theory; QM/MM, hybrid quantum mechanics/molecular mechanics.

■ REFERENCES

(1) Zámocký, M., Garcia-Fernandez, M. Q., Gasselhuber, B., Jakopitsch, C., Furtmüller, P. G., Loewen, P. C., Fita, I., Obinger, C., and Carpena, X. (2012) High thermal and conformational stability of secretory eukaryotic catalase-peroxidases - Answers from first crystal structure and unfolding studies. *J. Biol. Chem. 287*, 32254−32262.

(2) Gasselhuber, B., Carpena, X., Graf, M. M. H., Pirker, K. F., Nicolussi, A., Sündermann, A., Hofbauer, S., Zámocký, M., Furtmüller, P. G., Jakopitsch, C., Oostenbrink, C., Fita, I., and Obinger, C. (2015) Eukaryotic catalase-peroxidase: the role of the Trp-Tyr-Met adduct in protein stability, substrate accessibility, and catalysis of hydrogen peroxide dismutation. *Biochemistry 54*, 5425−5438.

(3) Yamada, Y., Fujiwara, T., Sato, T., Igarashi, N., and Tanaka, N. (2002) The 2.0 Å crystal structure of catalase-peroxidase from *Haloarcula marismortui*. *Nat. Struct. Biol. 9*, 691−695.

(4) Carpena, X., Loprasert, S., Mongkolsuk, S., Switala, J., Loewen, P. C., and Fita, I. (2003) Catalase-peroxidase KatG of *Burkholderia pseudomallei* at 1.7 Å resolution. *J. Mol. Biol. 327*, 475−489.

(5) Jakopitsch, C., Kolarich, D., Petutschnig, G., Furtmüller, P. G., and Obinger, C. (2003) Distal side tryptophan, tyrosine and methionine in catalase-peroxidases are covalently linked in solution. *FEBS Lett. 552*, 135−140.

(6) Donald, L. J., Krokhin, O. V., Duckworth, H. W., Wiseman, B., Deemagarn, T., Singh, R., Switala, J., Carpena, X., Fita, I., and Loewen, P. C. (2003) Characterization of the catalase-peroxidase KatG from *Burkholderia pseudomallei* by mass spectrometry. *J. Biol. Chem. 278*, 35687−35692.

(7) Bertrand, T., Eady, N. A., Jones, J. N., Jesmin, Nagy, J. M., Jamart-Grégoire, B., Raven, E. L., and Brown, K. A. (2004) Crystal structure of *Mycobacterium tuberculosis* catalase-peroxidase. *J. Biol. Chem. 279*, 38991−38999.

(8) Njuma, O. J., Ndontsa, E. N., and Goodwin, D. C. (2014) Catalase in peroxidase clothing: Interdependent cooperation of two cofactors in the catalytic versatility of KatG. *Arch. Biochem. Biophys. 544*, 27−39.

(9) Zámocký, M., Gasselhuber, B., Furtmüller, P. G., and Obinger, C. (2012) Molecular evolution of hydrogen peroxide degrading enzymes. *Arch. Biochem. Biophys. 525*, 131−144.

(10) Zámocký, M., Furtmüller, P. G., and Obinger, C. (2008) Evolution of catalases from bacteria to humans. *Antioxid. Redox Signaling 10*, 1527−1548.

(11) Zamocky, M., Furtmüller, P. G., and Obinger, C. (2010) Evolution of structure and function of class I peroxidases. *Arch. Biochem. Biophys. 500*, 45−57.

(12) Zámocký, M., Hofbauer, S., Schaffner, I., Gasselhuber, B., Nicolussi, A., Soudi, M., Pirker, K. F., Furtmüller, P. G., and Obinger, C. (2015) Independent evolution of four heme peroxidase superfamilies. *Arch. Biochem. Biophys. 574*, 108−119.

(13) Jakopitsch, C., Auer, M., Regelsberger, G., Jantschko, W., Furtmüller, P. G., Rüker, F., and Obinger, C. (2003) Distal site aspartate is important in the catalase activity of catalase-peroxidases. *Biochemistry 42*, 5292−5300.

(14) Zhao, X., Khajo, A., Jarrett, S., Suarez, J., Levitsky, Y., Burger, R. M., Jarzecki, A. A., and Magliozzo, R. S. (2012) Specific function of the Met-Tyr-Trp adduct radical and residues Arg-418 and Asp-137 in the atypical catalase reaction of catalase-peroxidase KatG. *J. Biol. Chem. 287*, 37057−37065.

(15) Regelsberger, G., Jakopitsch, C., Furtmüller, P. G., Rüker, F., Switala, J., Loewen, P. C., and Obinger, C. (2001) The role of distal tryptophan in the bifunctional activity of catalase-peroxidases. *Biochem. Soc. Trans. 29*, 99−105.

(16) Jakopitsch, C., Auer, M., Ivancich, A., Rüker, F., Furtmüller, P. G., and Obinger, C. (2003) Total conversion of bifunctional catalase-peroxidase (KatG) to monofunctional peroxidase by exchange of a conserved distal side tyrosine. *J. Biol. Chem. 278*, 20185−20191.

(17) Ghiladi, R. A., Medzihradszky, K. F., and Ortiz de Montellano, P. R. (2005) Role of the Met-Tyr-Trp cross-link in *Mycobacterium tuberculosis* catalase-peroxidase (KatG) as revealed by KatG (M255I). *Biochemistry 44*, 15093−15105.

(18) Ghiladi, R. A., Knudsen, G. M., Medzihradszky, K. F., and Ortiz de Montellano, P. R. (2005) The Met-Tyr-Trp cross-link in *Mycobacterium tuberculosis* catalase-peroxidase (KatG): autocatalytic formation and effect on enzyme catalysis and spectroscopic properties. *J. Biol. Chem. 280*, 22651−22663.

(19) Yu, S., Girotto, S., Zhao, X., and Magliozzo, R. S. (2003) Rapid formation of compound II and a tyrosyl radical in the Y229F mutant of *Mycobacterium tuberculosis* catalase-peroxidase disrupts catalase but not peroxidase function. *J. Biol. Chem. 278*, 44121−44127.

(20) Baker, R. D., Cook, C. O., and Goodwin, D. C. (2004) Properties of catalase-peroxidase lacking its C-terminal domain. *Biochem. Biophys. Res. Commun. 320*, 833−839.

(21) Wang, Y., and Goodwin, D. C. (2013) Integral role of the I′-helix in the function of the ″inactive″ C-terminal domain of catalase-

DOI: 10.1021/acs.biochem.6b00436
Biochemistry 2016, 55, 3528−3541

peroxidase (KatG). *Biochim. Biophys. Acta, Proteins Proteomics 1834*, 362−371.
(22) Kudalkar, S. N., Njuma, O. J., Li, Y., Muldowney, M., Fuanta, N. R., and Goodwin, D. C. (2015) A role for catalase-peroxidase large loop 2 revealed by deletion mutagenesis: control of active site water and ferric enzyme reactivity. *Biochemistry 54*, 1648−62.
(23) Jakopitsch, C., Wiseman, B., Vlasits, J., Loewen, P., and Obinger, C. (2007) Redox intermediates in the catalase cycle of catalase-peroxidase from *Synechocystis*, *Mycobacterium tuberculosis* and *Burkholderia pseudomallei*. *Biochemistry 46*, 1183−1193.
(24) Zhao, X., Suarez, J., Khajo, A., Yu, S., Metlitsky, L., and Magliozzo, R. S. (2010) A radical on the Met-Tyr-Trp modification required for catalase activity in catalase-peroxidase is established by isotopic labeling and site-directed mutagenesis. *J. Am. Chem. Soc. 132*, 8268−8269.
(25) Vidossich, P., Alfonso-Prieto, M., Carpena, X., Loewen, P. C., Fita, I., and Rovira, C. (2007) Versatility of the electronic structure of compound I in catalase-peroxidase. *J. Am. Chem. Soc. 129*, 13436−13446.
(26) Loewen, P. C., Carpena, X., Vidossich, P., Fita, I., and Rovira, C. (2014) An ionisable active-site tryptophan imparts catalase activity to a peroxidase core. *J. Am. Chem. Soc. 136*, 7249−7252.
(27) Kruft, B. I., Magliozzo, R. S., and Jarzecki, A. A. (2015) Density functional theory insights into the role of the methionine-tyrosine-tryptophan adduct radical in the KatG catalase reaction: O_2 release from the oxyheme intermediate. *J. Phys. Chem. A 119*, 6850−6866.
(28) Derat, E., Cohen, S., Shaik, S., Altun, A., and Thiel, W. (2005) Principle active species of horseradish peroxidase compound I: a hybrid quantum mechanical/molecular mechanical study. *J. Am. Chem. Soc. 127*, 13611−13621.
(29) Bassan, A., Blomberg, M. R. A., Borowski, T., and Siegbahn, P. E. M. (2006) Theoretical studies of enzyme mechanisms involving high-valent iron intermediates. *J. Inorg. Biochem. 100*, 727−743.
(30) Vlasits, J., Jakopitsch, C., Schwanninger, M., Holubar, P., and Obinger, C. (2007) Hydrogen peroxide oxidation by catalase-peroxidase follows a non-scrambling mechanism. *FEBS Lett. 581*, 320−324.
(31) Vlasits, J., Jakopitsch, C., Bernroitner, M., Zamocky, M., Furtmüller, P. G., and Obinger, C. (2010) Mechanisms of catalase activity of heme peroxidases. *Arch. Biochem. Biophys. 500*, 74−81.
(32) Carpena, X., Wiseman, B., Deemagarn, T., Singh, R., Switala, J., Ivancich, A., Fita, I., and Loewen, P. C. (2005) A molecular switch and electronic circuit modulate catalase activity in catalase-peroxidases. *EMBO Rep. 6*, 1156−1162.
(33) Jakopitsch, C., Schmuckenschlager, F., Wanasinghe, A., Furtmüller, P. G., Rüker, F., Ivancich, A., and Obinger, C. (2004) Influence of the unusual covalent adduct on the kinetics and formation of radical intermediates in *Synechocystis* catalase-peroxidase: a stopped-flow and EPR characterization of the Met275, Tyr249 and Arg439 variants. *J. Biol. Chem. 279*, 46082−46095.
(34) Carpena, X., Wiseman, B., Deemagarn, T., Herguedas, B., Ivancich, A., Singh, P. C., Loewen, P. C., and Fita, I. (2006) Roles for Arg426 and Trp111 in the modulation of NADH oxidase activity of the catalase-peroxidase KatG from *Burkholderia pseudomallei* inferred from pH-induced structural changes. *Biochemistry 45*, 5171−5179.
(35) Zamocky, M., Furtmüller, P. G., and Obinger, C. (2009) Two distinct groups of fungal catalase-peroxidases. *Biochem. Soc. Trans. 37*, 772−777.
(36) Zamocky, M., Droghetti, E., Bellei, M., Furtmüller, P. G., Gasselhuber, B., Pabst, M., Battistuzzi, G., Smulevich, G., and Obinger, C. (2012) Eukaryotic extracellular catalase-peroxidase from *Magnaporthe grisea* − biophysical/chemical characterization of the first representative from a novel phytopathogenic KatG Group. *Biochimie 94*, 673−683.
(37) Schmid, N., Christ, C. D., Christen, M., Eichenberger, A. P., and van Gunsteren, W. F. (2012) Architecture, implementation and parallelisation of the GROMOS software for biomolecular simulation. *Comput. Phys. Commun. 183*, 890−903.
(38) Schmid, N., Eichenberger, A. P., Choutko, A., Riniker, S., Winger, M., Mark, A. E., and van Gunsteren, W. F. (2011) Definition and testing of the GROMOS force-field versions 54A7 and 54B7. *Eur. Biophys. J. 40*, 843−856.
(39) Aqvist, J., Medina, C., and Samuelsson, J. E. (1994) A new method for predicting binding affinity in computer-aided drug design. *Protein Eng., Des. Sel. 7*, 385−391.
(40) Åqvist, J., Luzhkov, V. B., and Brandsdal, B. O. (2002) Ligand binding affinities from MD simulations. *Acc. Chem. Res. 35*, 358−365.
(41) Graf, M. M. H., Sucharitakul, J., Bren, U., Chu, D. B., Koellensperger, G., Hann, S., Furtmüller, P. G., Obinger, C., Peterbauer, C. K., Oostenbrink, C., Chaiyen, P., and Haltrich, D. (2015) Reaction of pyranose dehydrogenase from *Agaricus meleagris* with its carbohydrate substrates. *FEBS J. 282*, 4218−4241.
(42) Banerjee, S., Zamocky, M., Furtmüller, P. G., and Obinger, C. (2010) Probing the two-domain structure of homodimeric prokaryotic and eukaryotic catalase-peroxidases. *Biochim. Biophys. Acta, Proteins Proteomics 1804*, 2136−2145.
(43) Fita, I., Carpena, X., and Loewen, P. C. (2016) Catalase-peroxidase (KatG) structure and function. In *Heme Peroxidases* (Raven, E., and Dunford, B., Eds.) pp 135−155, Royal Society of Chemistry, Cambridge, U.K.
(44) Gasselhuber, B., Jakopitsch, C., Zamocky, M., Furtmüller, P. G., and Obinger, C. (2016) Mechanistic aspects of catalase-peroxidase. In *Heme Peroxidases* (Raven, E., and Dunford, B., Eds.) pp 156−180, Royal Society of Chemistry, Cambridge, U.K.
(45) Baker, R. D., Cook, C. O., and Goodwin, D. C. (2006) Catalase-peroxidase active site restructuring by a distant and ″inactive″ domain. *Biochemistry 45*, 7113−7121.
(46) Poulos, T. L. (2016) Cytochrome c peroxidase-cytochrome c complexes. In *Heme Peroxidases* (Raven, E., and Dunford, B., Eds.) pp 31−46, Royal Society of Chemistry, Cambridge, U.K.
(47) Wiseman, B., Colin, J., Smith, A. T., Ivancich, A., and Loewen, P. C. (2009) Mechanistic insight into the initiation step of the reaction of *Burkholderia pseudomallei* catalase-peroxidase with peroxyacetic acid. *JBIC, J. Biol. Inorg. Chem. 14*, 801−811.
(48) Ivancich, I., Donald, L. J., Villanueva, J., Wiseman, B., Fita, I., and Loewen, P. C. (2013) Spectroscopic and kinetic investigations of the reactions of peroxoacetic acid with *Burkholderia pseudomallei* catalase-peroxidase, KatG. *Biochemistry 52*, 7271−7282.
(49) Santoni, E., Jakopitsch, C., Obinger, C., and Smulevich, G. (2004) Manipulating the covalent link between distal side tryptophan, tyrosine and methionine in catalase-peroxidases: an electronic absorption and resonance Raman study. *Biopolymers 74*, 46−50.
(50) Miller, M. A., Shaw, A., and Kraut, J. (1994) 2.2 A structure of oxy-peroxidase as a model for the transient enzyme: peroxide complex. *Nat. Struct. Biol. 1*, 524−531.
(51) Marquez, L. A., Quitoriano, M., Zilinskas, B. A., and Dunford, H. B. (1996) Kinetic and spectral properties of pea cytosolic ascorbate peroxidase. *FEBS Lett. 389*, 153−156.
(52) Vlasits, J., Furtmüller, P. G., Jakopitsch, C., Zamocky, M., and Obinger, C. (2010) Probing hydrogen peroxide oxidation kinetics of wild-type *Synechocystis* catalase-peroxidase (KatG) and selected variants. *Biochim. Biophys. Acta, Proteins Proteomics 1804*, 799−805.

DOI: 10.1021/acs.biochem.6b00436
Biochemistry 2016, 55, 3528−3541